MATERIALE PLASTICE
https://revmaterialeplastice.ro
https://doi.org/10.37358/Mat.Plast.1964

Impact of Aligned Carbon Nanotubes on the Mechanical Properties and Sensing Performance of EVA/CNTs Composites

JILONG TANG[1], CHENG LIN[1], CHUNMEI DUAN[2], LIN NIE[3], LEI HAN[1]*
[1] School of Automobile and Transportation Engineering, Guangdong Polytechnic Normal University, West Zhongshan Road, No. 293, 510665, Guangzhou, China
[2] School of Mechanical Engineering, Guangdong Ocean University, Zhanjiang, East Jiefang Road, No.40, 524025, Zhanjiang, China
[3] School of Mechatronics and Vehicle Engineering, East China Jiaotong University, Nanchang, Eastern Street of Shuanggang, No.808, 330013, Nanchang, China

***Abstract**: This study investigated the mechanical and sensing properties of ethylene-vinyl acetate (EVA)/carbon nanotubes (CNTs) composites in both film and fiber forms. The incorporation of aligned CNTs in the composite fibers possess improved mechanical properties and enhanced sensing performance compared to those of composite films with randomly dispersed CNTs. Thermogravimetric analysis revealed promising thermal stability, indicating potential applications for long-term usage. Cyclic tensile testing demonstrated that the fiber samples with better CNT alignment exhibit higher sensitivity, emphasizing the significance of CNT orientation in constructing an efficient conductive network for strain sensing. Considering the contribution of the CNTs' orientation along the measuring direction, a model contains modification parameters was proposed, where a master curve was given, revealing the ideal potential of the EVA/CNTs composite fiber with perfectly aligned CNTs. This work provides valuable insights into the influence of CNT alignment on the mechanical and sensing properties of EVA/CNTs composites. The results underscore the importance of optimizing CNT orientation for enhanced sensing performance in various engineering applications.*

***Keywords:** ethylene-vinyl acetate, carbon nanotubes, orientation, strain sensor*

1. Introduction

Carbon nanotubes (CNTs) have garnered significant attention in recent years due to their exceptional mechanical, electrical, and thermal properties [1-6]. The integration of CNTs into polymer matrices has promoted the development of novel composite materials with enhanced functionalities, making them become promising candidates for various engineering applications, including strain sensing [7-11].

Among these composite materials, the combination of ethylene-vinyl acetate (EVA) copolymer and CNTs has shown great potential for various applications [12-18]. Firstly, due to its electromagnetic shielding properties and conductivity, the EVA/CNTs composite material can be utilized in the manufacturing of electronic devices, communication equipment, and aerospace components to effectively shield electromagnetic interference [12-14]. Secondly, through the utilization of its sensing capabilities, the EVA/CNTs composite material can be applied in the field of flexible sensors for monitoring pressure, tension, and other physical parameters, widely used in medical, health monitoring, and smart wearable devices [15, 16]. Furthermore, by adjusting the orientation of CNTs, control over the mechanical properties can be achieved, enabling shape memory or deformation capabilities, which can be applied in the fields of smart structures, aerospace, and adaptive materials [17, 18]. In summary, the EVA/CNTs composite material has potential applications in multiple fields, bringing innovation and benefits to industries such as electronics, sensors, smart materials, environmental monitoring, and energy storage.

In this context, the orientation of CNTs in the composite materials are critical factors influencing their mechanical and sensing properties. The alignment of CNTs in the composite structure is known to enhance the mechanical strength and electrical conductivity. In EVA/CNTs composites, the CNTs can form conductive pathways along the direction of applied stress, leading to improved electrical response during deformation [15, 19 - 22]. Consequently, it becomes essential to investigate the effects of CNT

**email: hanlei@gpnu.edu.cn*

alignment on the mechanical and sensing performance of EVA/CNTs composites.

To the best of our knowledge, few studies have focused on the impact of CNT alignment on the mechanical and strain sensoring behaviour of the EVA/CNTs composites. Therefore, in this study, we investigated two different forms of EVA/CNTs composite materials, which are composite films with randomly dispersed CNTs and composite fibers with highly oriented CNTs, in order to compare their behavior under different loading conditions. Mophological study and thermal analysis were performed to evaluate the dispersion of the CNTs and the thermal stability of the composites, respectively. The mechanical properties were also investigated, where a methemtical modelling considering the contribution of the CNTs' orientation along the measuring direction was suggested. To assess the strain sensing capabilities, the relative change in resistivity (RCR) value was employed, and its relationship with time was studied using a mathematical formula. The research results of this study will provide valuable insights into the design and optimization of strain sensors based on EVA/CNT composite materials. Understanding the impact of CNT alignment on the mechanical and sensing properties will facilitate the development of more efficient and reliable strain sensors for a wide range of applications.

2. Materials and methods

2.1. Preparation of EVA/CNTs composites

The Ethylene-vinyl acetate (EVA) copolymer employed in this study was sourced as Elvax 265 from DuPont, possessing a vinyl acetate (VA) content of 28 wt.% and a melt flow index (MFI) of 3 at 190ºC/2.16 kg. The carbon nanotubes (SWCNTs, Signis® SG65i) were supplied by Sigma Aldrich (Shanghai) Trading Co., Ltd., with a median length of 1 μm, and a diameter in average of 0.78 nm. Both the polymer granules and CNTs powder were subjected to vacuum oven drying at 60ºC for 48h to ensure complete removal of moisture.

Subsequently, the designated proportion of the EVA and 2 wt.% CNTs were loaded into a 1-Liter kneader (KNEADER MACHINERY CO., LTD, Taiwan) at 60 rpm and 120ºC for 10 min. The blended composite was pelletized into granules, and stored in a dehydrated and oxygen-free environment for further experiment. For comparision, the neat EVA granules without CNTs were also kneaded and pelletized, which are named as ***k-EVA*** in this study.

The EVA/CNTs granules were then prepared into composite films and composite fibers, respectively (Figure 1). The composite films with a thickness of 1 mm were prepared using a vacuum hot press (Zhengzhou Craftsman Machinery Equipment Co., Ltd, K-001) at a temperature of 110ºC and under a pressure of 500 N for 20 min. The obtained films were then cut into specimens of size 14 cm×1 cm for further mechanical testing. For the composite fibers, a a co-rotating twin-screw extruder (Leistritz Micro-18/GL-40D) operating at 60 rpm and 120ºC was utilized with a die of 2 m diameter. A spinning wheel was equipped in order to strech the melt filament into composite fibers with a diameter of 1 mm. Subsequently, these filaments were cut into 14cm long for mechanical evalation. Besides, the ***k-EVA*** granules as well as the virgin EVA granules (***v-EVA***) without any treatment were also prepared into the films and fibers using the same processing procedure above, respectively.

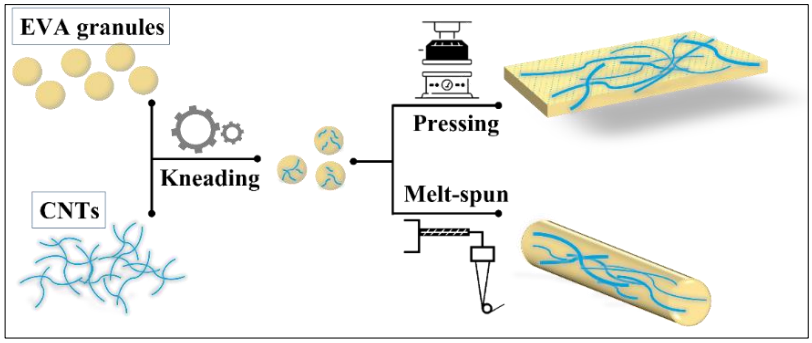

Figure 1. Schematic depiction of the fabrication procedure to produce the EVA/CNTs film and fibers

2.2. Characterization of EVA/CNTs composites

The fracture section and surface morphology of the EVA/CNTs composite membranes were examined using scanning electron microscopy (SEM, Carl Zeiss Microscopy, Germany) at an accelerating voltage of 10 kV. Before testing, the samples were sputter-coated with an ultrathin Au layer to enhance microstructural observation.

Thermal degradation behavior of the EVA/CNTs composite as well as the neat EVA were determined using a Thermal Gravimetric Analyzer (TGA, Pyris 1, USA). The measurements were conducted under a nitrogen atmosphere with a temperature rise rate of 10 K/min up to 1000°C.

The mechanical properties of EVA/CNTs composite were evaluated using a tensile testing machine (Shenzhen SUNS Technology Stock Co. Ltd, EUT5105), connected to a Keithley 6487 Pico-ammeter. All the EVA/CNTs composite specimens were securely clamped with insulated fixtures with a gauge length of 10 cm and stretched uniaxially at a speed of 2 mm/min until fracture, facilitating the correlation between input strain and measured resistance. Synchronous recording of mechanical properties and electrical behavior during the stretching process provides a comprehensive evaluation of the electro-mechanical properties of the specimens. At least 5 specimens under each experimental condition were tested to ensure result reproducibility.

3. Results and discussions

3.1. SEM morphologies

Figure 2 displays the morphology of the EVA/CNTs films and fibers, respectively. In Figure 2a, the SEM image of the EVA/CNTs composite film reveals a random orientation of CNTs dispersed throughout the EVA matrix. The CNTs appear to be distributed in various directions, without a specific alignment pattern. The composite membrane exhibits a homogeneous microstructure, and the CNTs are evenly distributed within the EVA matrix. In Figure 2b, however, a distinct alignment of CNTs is observed along the longitudinal axis of the fiber. This aligned configuration of CNTs indicates an anisotropic structure within the composite fiber, characterized by the preferential alignment of CNTs during the extrusion process.

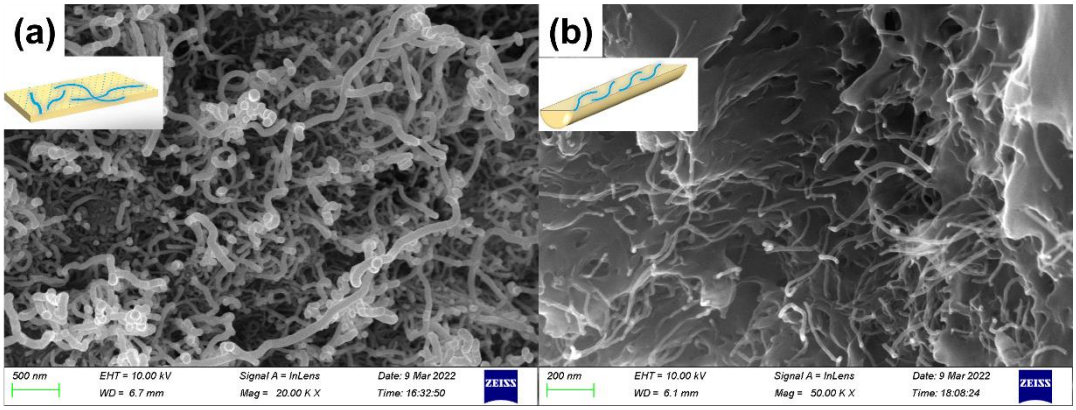

Figure 2. Morphologies of (a) the isotropic CNTs in EVA/CNTs composite films and (b) the aligned CNTs in EVA/CNTs composite fibers

3.2. Thermal gravity analysis of the EVA/CNTs composites

The thermal analysis results of the two samples, namely the neat EVA (***v-EVA***) and the EVA/CNTs granules, acquired from thermogravimetric analysis, are depicted in Figure 3. The thermal behavior of ***k-EVA*** prepared by the kneader exhibits substantial similarity with the ***v-EVA*** and is, therefore, not presented herein.

Nevertheless, even for the EVA/CNTs with 2 wt.% CNTs loading, marginal deviations from the EVA are observed, suggesting that the melt mixing procedure and the selected CNTs particles exert minimal influence on the EVAs thermal behavior. Regarding the TGA results, both samples demonstrate

a single-step degradation pattern. Initial mass loss occurs within the temperature range of 420ºC to 450ºC. During this stage, the heat flow rate remains relatively constant, indicating a gradual decomposition process. The derivative mass curve exhibits a corresponding peak, indicating the maximum rate of mass loss during this step. Subsequently, the derivative mass curve displays a sharp peak, signifying a rapid rate of mass loss. The TGA results, along with the corresponding heat flow rate and derivative mass curves, offer clear insights into the thermal stability and decomposition behavior of both the neat EVA and the EVA/CNTs composite.

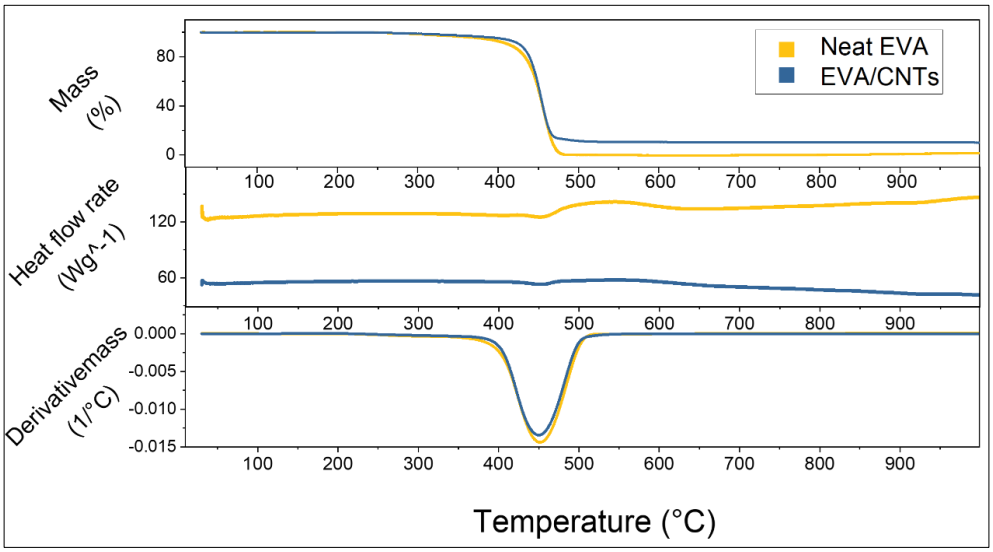

Figure 3. a. TGA, b. DSC and c. DTG curve of the sample neat EVA and the EVA/CNTs

3.3. Mechanical properties of the EVA/CNTs composite films and fibers

The stress-strain curves of six specimens are shown in Figure 4a, and the detailed Young's modules as well as the corresponding eloangation at break of all the specimen are shown in Figure 4b. It should be noted that: (1) Among all the three materials (EVA/CNTs composite shown in blue, ***v-EVA*** shown in yellow, ***k-EVA*** shown in red), the EVA/CNTs composite exhibits the highest strength and the lowest elongation at break, followed by the ***v-EVA***, while the ***k-EVA*** displays the lowest strength and the highest elongation at break (2). For each material type, the strength of the fiber is consistently higher than that of the film. This phenomenon can be attributed to the melt spinning process. Under the action of shear forces during the melt spinning, both the polymer chains and internal CNTs tend to align along the spinning direction, thereby reinforcing the axial force transmission. In particular, the orientation of CNTs forms a nano-spring structure, effectively enhancing the axial load-carrying capacity.

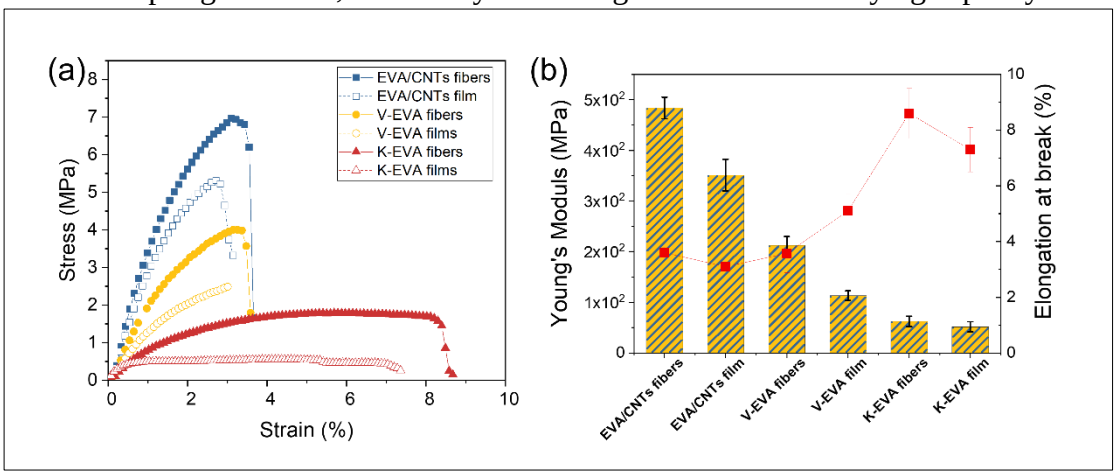

Figure 4. a) Stress-strain curve and b) comparison of Young's modulus and elongation at break of EVA/CNTs, *v-EVA* and *k-EVA*

Moreover, it is imperative to assess material durability and reliability under cyclic loading conditions to comprehensively evaluate the mechanical performance through cyclic tensile testing. The cyclic measurement results of the EVA/CNTs composite fibers, subjected to 20 cycles of stretching-recovery at a constant speed of 4mm/min up to a 2mm displacement, are depicted in Figure 5a, with the initial cycle highlighted in red. In each cycle's stress-strain curve, the area under the corresponding curves during both the stretching and recovery processes represents the energy required for each respective process. The difference between these integrated areas, which corresponds to the dissipated energy during the stretching and recovery processes, is illustrated in Figure 5b. Dissipated energy ***E*** refers to the energy converted into heat or other forms during the material's deformation and fracture processes (1). It serves as a quantifiable measure of the material's capacity to dissipate energy and endure repeated loading without experiencing catastrophic failure [23-25].

$$E = \int \sigma(t) d\epsilon(t) = S_{stretching} - S_{releasing} \quad (1)$$

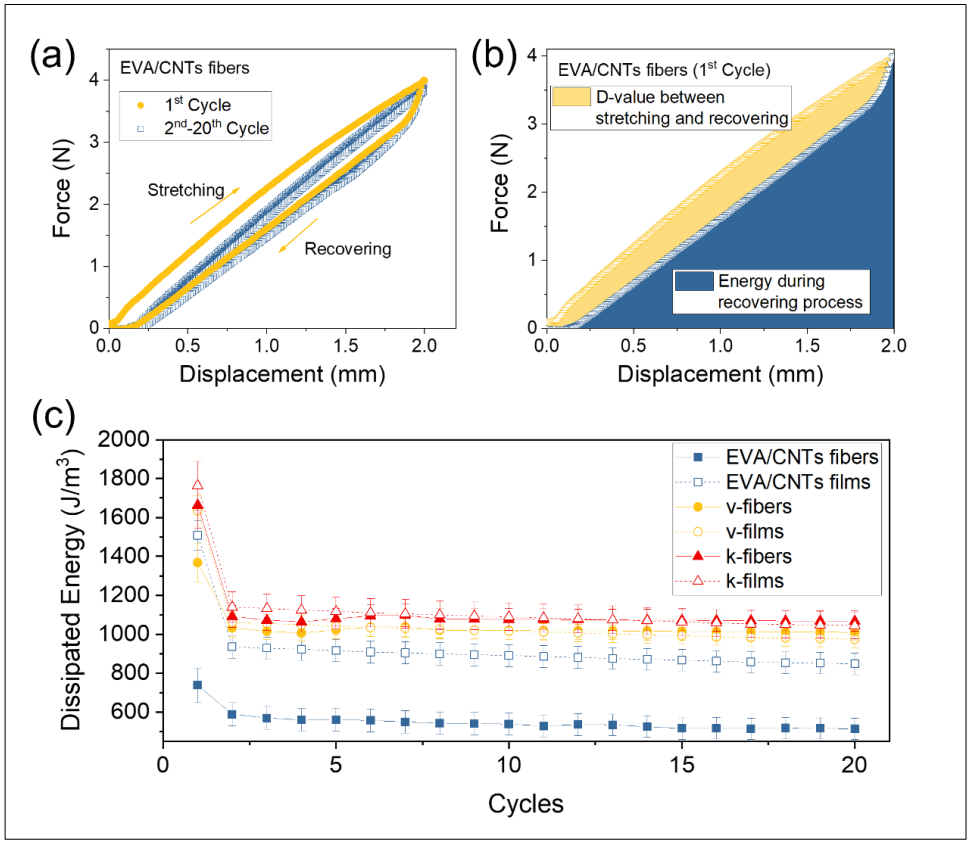

Figure 5. a. The stress-strain curves of EVA/CNT composite fibers measured under cyclic loading conditions. b. The first cycle of stretching and releasing with the yellow region representing the dissipated energy (***E***). c. The relationship between dissipated energy and the number of cycles for the six different specimens

The Figure 5c presents the dissipated energy of the six specimens over 20 cycles, subjected to a strain up to 2%. For each specimen, the dissipated energy reaches its highest value in the first cycle, followed by a notable decline starting from the second cycle, eventually reaching a stabilized state. These observations suggest that all the specimens exhibit considerable potential for prolonged applications. Furthermore, within each cycle, the dissipated energy of the fibers decreases comparing with that of the films prepared using the identical material, attributable to the influence of shear stress on the molecular chains and the CNTs during the melt spinning process. Notably, the sample fiber with high orientation of carbon nanotubes exhibits the lowest dissipated energy. However, this is attributed to the spiral shape

of the carbon nanotubes, which tend to unwind during the sample's stretching process, thereby storing a portion of energy. This stored energy is subsequently released during the sample's recovery process, effectively playing the role of a nano-spring that stores latent energy.

Despite the high orientation achieved by CNTs within the composite fiber, the average angle between the CNTs and the fiber axis direction <γ> is not zero. Therefore, for an accurate calculation of the dissipated energy *E*, one must take into account the contribution of CNTs along the fiber axis direction, as represented in equation 2:

$$E_{modified} = E \cdot cos < \gamma > \quad (2)$$

For the hot-pressed EVA/CNTs film in this study, the orientation distribution of the CNTs was uniformly dispersed in the plane of the film, which is, randomly dispersed in the range of 360°. Therefore, the CNTs orientation between the direction of the melt spun fibers cos<γ> could be calculated using equation 3 [26, 27]:

$$cos_{film} < \gamma >= \frac{\int_0^{\pi/2} cos\gamma \cdot d\gamma}{\int_0^{\pi} d\gamma} = \frac{1}{\pi} \approx 0.318 \quad (3)$$

Figure 6 shows the measured dissipated energy *E* of the EVA/CNTs film and fibers using hollow symbols in green and blue, respectively. Using the equation 2 and 3, the modified dissipated energy of the hot-pressed EVA/CNTs film with isotropic CNTs are presented in solid symbols, where all the CNTs are assumed to be totally aligned. Through interpolation adjustments, assuming a perfect orientation of CNTs within the EVA/CNTs composite fiber, the resulting value of cos_{fiber}<γ> is obtained as 0.531. This indicates that CNTs within the composite fiber exhibit higher alignment along the extrusion direction of the composite fiber, and CNTs as nano-springs, their contribution relative to CNTs in films increases by approximately 67%.

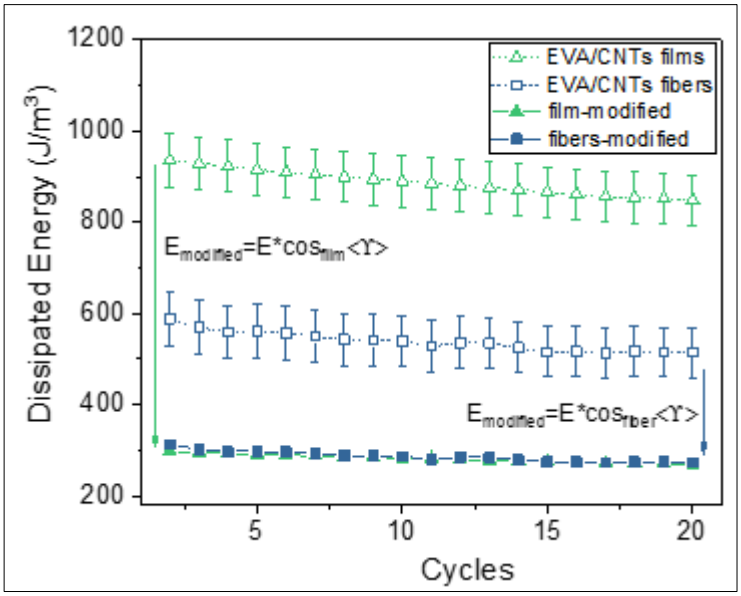

Figure 6. The measured dissipated energy of the EVA/CNTs films (hollow triangle in green) and fibers (hollow square in blue), the mastered modified dissipated energy considering the contribution of the aligned CNTs (solid symbols) using equation 2

3.4. Strain sensing behavior of the EVA/CNTs composite films and fibers

Figure 7a presents the correlation between the relative change of resistance (RCR value) and strain in the EVA/CNTs composite films and fibers in green and blue, respectively. The sensitivity coefficient

of a sample can be expressed as the Gauge Factor (GF), which signifies the change in resistance concerning the applied strain. The GF is defined as the ratio of the relative resistance to the applied strain and serves as a measure to determine the sensor's sensitivity. Typically, GF is dependent on the strain and can be calculated as follows [28-30]:

$$\boldsymbol{GF} = \frac{\boldsymbol{d(RCR)}}{\boldsymbol{d\varepsilon}} = \frac{\boldsymbol{d[(R_t - R_0)/R_0]}}{\boldsymbol{d\varepsilon}} \tag{4}$$

As indicated in Figure 7a, the maximal GF of the EVA/CNTs films and fibers are obtained as 74.3 and 362.5, respectively. From a physics perspective, GF is determined by the degree of nanoparticles dispersion under the same tensile distance, which corresponds to the level of disruption in the constructed conductive network. Therefore, for isotropic CNTs within the film, stretching merely results in the separation of particles in the stretching direction, with little impact on the network deformation in other dimensions. However, for the better-aligned CNTs within the fiber, stretching leads to a greater distance between the CNTs, resulting in a more pronounced increase in resistance and, consequently, achieving higher GF.

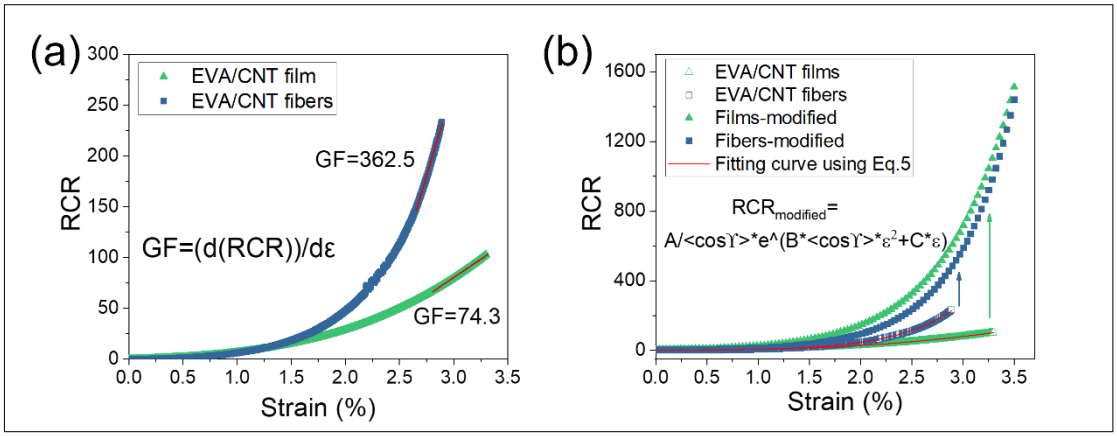

Figure 7. a. Relative change in resistivity (RCR) as a function of the applied strain on the EVA/CNTs films (green) and fibers (blue); b. the modified RCR curve considering totally aligned CNTs in films and fibers using equation 6

The RCR value of the specimen indicates the alteration in the electrical signal of the specimens during stretching, which can be quantified using equation 5, which is based on the tunneling theory and multi-steps of simplification [31-35]:

$$RCR = A \cdot exp[B\varepsilon^2 + C\varepsilon] \tag{5}$$

The fitting curve using equation 5 are presented in red in Figure 7b. Considering the contribution of CNTs' orientation in the constructed conductive network, equation 6 is proposed. Applying which, the RCR curves in hollow symbols can be adjusted. The resulting curve represents the theoretical RCR curve when CNTs achieve perfect alignment. Since the two modified curves are separately calculated for films and fibers, and given their highly similar characteristics after modification, this further validates the reasonableness of our proposed assumption.

$$RCR_{modified} = \frac{A}{cos\gamma} \cdot exp[B \cdot cos\gamma \cdot \varepsilon^2 + C\varepsilon] \tag{6}$$

Based on our assumption, the samples of films and fibers should be primarily determined by the involvement of different CNTs in the construction of the conductive network used for sensing purposes.

Therefore, we conducted a study with minimal strain to investigate their sensing performance under repeated stretching cycles. Figure 8a illustrates the RCR values of the two samples over ten cycles. It is worth noting that the RCR performance in the first cycle differs from the subsequent cycles. This discrepancy is attributed to the interface interaction between the polymer resin and CNTs, which is a common reason for adopting "pre-stretching" in many strain sensors before application.

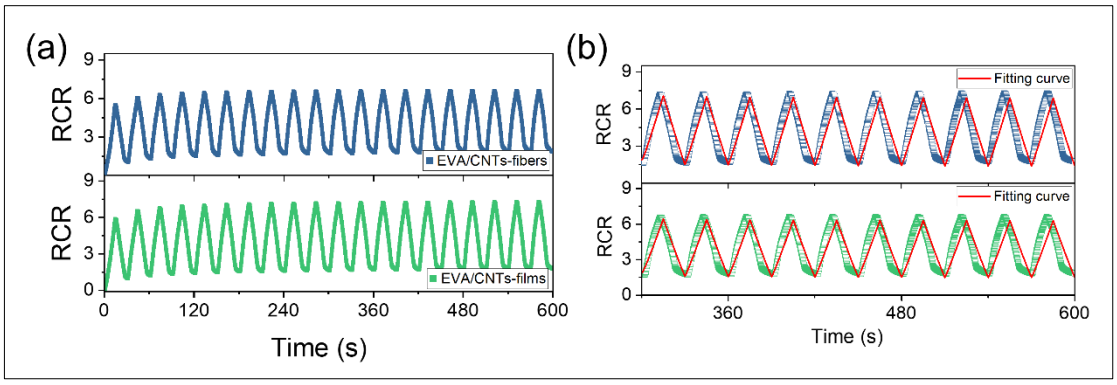

Figure 8. a. RCR value as a function of time for the EVA/CNTs composite fibers (blue) and films (green) for 20 cycles; b. The detailed data and the fitting curve (red) using equation 7 for the 11th-20th cycles

The RCR value of the strain sensor is commonly examined over cyclic measurements as a function of time using equation 7 [36, 37]:

$$\boldsymbol{RCR = \frac{2A}{\pi}\left(\left|arcsin\left(sin\frac{2\pi t}{p}\right)\right|^{n} + \omega\left(\frac{t}{10p}\right)^{C}\right) \times e + f} \quad (7)$$

where $\boldsymbol{A}$ represents the initial amplitude, corresponding to the maximum RCR value observed in the first cycle, while $\boldsymbol{P}$ denotes the duration of two cycles. The variables $\boldsymbol{\omega}$ and $\boldsymbol{C}$ are local parameters, reliant on the fundamental physical properties of the material. Additionally, $\boldsymbol{e}$ and $\boldsymbol{f}$ are two adjustable parameters, typically influenced by the parameter settings of the testing instrument.

As shown in Figure 8b, the presented data was taken from the 11th-20th cycles in Figure 8a. The experimental data was fitted in red curves using mathematical equation to obtain a quantitative model describing the relationship between the RCR and the measuring time for each specimen. The parameter results are presented in Table 1. The Pearson correlation coefficient for the two sets of parameters is 0.9999, indicating a high degree of similarity. The main discrepancy lies in parameter $\boldsymbol{A}$, representing the maximum RCR value in the first cycle. The specific relationship between parameter $\boldsymbol{A}$ and the physical significance of the alignment of CNTs cos<γ> is left for future investigation.

Table 1. The fitting parameters using equation 7 to describe the strain sensing behavior of both kind of specimens

Fitting parameters	Fibers	Films
A	5.39	4.68
P	60	60
n	1.04	1.06
ω	1.34	1.45
C	-0.03	-0.03
e	1	1
f	0	0

4. Conclusions

This study focused on the investigation of the mechanical and sensing properties of EVA/CNTs composite materials in both film and fiber forms. The composite fibers with aligned CNTs demonstrated enhanced mechanical properties and sensing performance compared to those of the composite films with random dispersion CNTs. In addition to the mophological study and the thermal behaviour, the mechanical properties of both EVA/CNTs composite fibers and films were also investigated. Additionally, cyclic tensile testing revealed that the fiber samples with better CNT alignment exhibited higher sensitivity, emphasizing the significance of CNT orientation in constructing the conductive network for strain sensing. Most importantly, a methemtical model considering the contribution of the CNTs' orientation along the measuring direction was suggested, resulting in a master curve revealing the modified dissipated energy. To evaluate the sensing performance under different conditions, the relationship between RCR and time was examined using a mathematical formula, where a master curve was also presented, demonstrating the correlation between the composite fibers and the films. Furthermore, the obtained parameters from fitting the film-shaped and the fiber-shaped specimens during the cyclic sensing measurement were highly similar, with a Pearson correlation coefficient of 0.9999. This discrepancy may be associated with the physical significance of $<\cos \gamma>$, which deserves further investigation in future research. Overall, our findings provide valuable insights into the influence of CNT alignment and dispersion on the mechanical and sensing properties of EVA/CNTs composite materials. The obtained results contribute to a better understanding of the potential applications of these materials in strain sensing and highlight the importance of optimizing CNT orientation for enhanced sensing performance in various engineering applications.

Acknowledgement: The authors appreciate the financial support from the Start-up funding Project from GPNU (No. 2021SDKYA061).

References

1.MAHESWARAN, R., SHANMUGAVEL, B. P., (2022), A critical review of the role of carbon nanotubes in the progress of next-generation electronic applications, Journal of Electronic Materials, 51(6), 2786-2800.
2.GULATI, S., KUMAR, S., GOYAL, K., ARORA, A., VARMA, R. S., (2022), Improving the air quality with Functionalized Carbon Nanotubes: Sensing and remediation applications in the real world. Chemosphere, 299, 134468.
3.HE, Y., ZHOU, M., MAHMOUD, M. H. H., LU, X., HE, G., ZHANG, L., ... AZAB, I. H. E., (2022), Multi-functional wearable strain/pressure sensor based on conductive carbon nanotubes/silk nonwoven fabric with high durability and low detection limit. Advanced Composites and Hybrid Materials, 5(3), 1939-1950.
4.ZHU, G., LI, H., PENG, M., ZHAO, G., CHEN, J., ZHU, Y., (2022), Highly-stretchable porous thermoplastic polyurethane/carbon nanotubes composites as a multimodal sensor, Carbon, 195, 364-371.
5.WU, B., YEASMIN, S., LIU, Y., CHENG, L. J., (2022), Sensitive and selective electrochemical sensor for serotonin detection based on ferrocene-gold nanoparticles decorated multiwall carbon nanotubes. Sensors and Actuators B: Chemical, 354, 131216.
6.LIU, C., TAN, Q., DENG, Y., YE, P., KONG, L., MA, X., ... LIU, B., (2022), Highly sensitive and stable 3D flexible pressure sensor based on carbon black and multi-walled carbon nanotubes prepared by hydro-thermal method, Composites Communications, 32, 101178.
7.YAMADA, T., HAYAMIZU, Y., YAMAMOTO, Y., YOMOGIDA, Y., IZADI-NAJAFABADI, A., FUTABA, D. N., HATA, K., (2011), A stretchable carbon nanotube strain sensor for human-motion detection, Nature nano-technology, 6(5), 296-301.
8.KANG, I., SCHULZ, M. J., KIM, J. H., SHANOV, V., SHI, D., (2006), A carbon nanotube strain sensor for structural health monitoring. Smart materials and structures, 15(3), 737.

9.WEI, Q., YI-LAN, K., ZHEN-KUN, L., QING-HUA, Q., QIU, L., (2009), A new theoretical model of a carbon nanotube strain sensor, Chinese Physics Letters, 26(8), 080701.
10.OBITAYO, W., LIU, T., (2012), A review: Carbon nanotube-based piezoresistive strain sensors, Journal of Sensors, 2012.
11.CHOI, G., JANG, H., OH, S., CHO, H., YOO, H., KANG, H. I., ... LEE, H. S., (2019), A highly sensitive and stress-direction-recognizing asterisk-shaped carbon nanotube strain sensor, Journal of Materials Chemistry C, 7(31), 9504-9512.
12.LI, Z., QI, X., XU, L., LU, H., WANG, W., JIN, X., ... DONG, Y., (2020), Self-repairing, large linear working range shape memory carbon nanotubes/ethylene vinyl acetate fiber strain sensor for human movement monitoring, ACS Applied Materials & Interfaces, 12(37), 42179-42192.
13.XIE, M., LI, S., QI, X., CHI, Z., SHEN, L., ISLAM, Z., DONG, Y., (2022), Thermal and infrared light self-repairing, high sensitivity, and large strain sensing range shape memory MXene/CNTs/EVA composites fiber strain sensor for human motion monitoring, Sensors and Actuators A: Physical, 347, 113939.
14.ROSCULET, R. T., STAN, F., FETECAU, C., On the strain sensing of EVA/MWCNT composite, *Mater. Plast.* **55**(3), 2018, 274-278
15.QU, M., FANG, J., MU, C., LI, Y., HUANG, S., HAN, L., ... QIN, Y., (2022), A novel study on the sandwich-structure strain sensor using ethylene-vinyl acetate-based hot-melt adhesive mesh web: Fabrication, properties, and modeling, Journal of Applied Polymer Science, 139(48), e53209.
16.ZHAO, J., DAI, K., LIU, C., ZHENG, G., WANG, B., LIU, C., ... SHEN, C., (2013), A comparison between strain sensing behaviors of carbon black/polypropylene and carbon nanotubes/polypropylene electrically conductive composites, Composites Part A: Applied Science and Manufacturing, 48, 129-136.
17.WANG, Z., HUANG, Y., SUN, J., HUANG, Y., HU, H., JIANG, R., ... ZHI, C., (2016), Polyurethane/ cotton/carbon nanotubes core-spun yarn as high reliability stretchable strain sensor for human motion detection, ACS applied materials & interfaces, 8(37), 24837-24843.
18.QIU, A., LI, P., YANG, Z., YAO, Y., LEE, I., MA, J., (2019), A path beyond metal and silicon: polymer/nanomaterial composites for stretchable strain sensors, Advanced Functional Materials, 29(17), 1806306.
19.ZHANG, Z. X., WANG, W. Y., YANG, J. H., ZHANG, N., HUANG, T., WANG, Y., (2016), Excellent electro-active shape memory performance of EVA/PCL/CNT blend composites with selectively localized CNTs, The Journal of Physical Chemistry C, 120(40), 22793-22802.
20. CHANG, B. P., KASHCHEEV, A., VEKSHA, A., LISAK, G., GOEI, R., LEONG, K. F., ... LIPIK, V., (2023), Nanocomposite foams with balanced mechanical properties and energy return from EVA and CNT for the midsole of sports footwear application, Polymers, 15(4), 948.
21.YE, L., WU, Q., QU, B., (2009), Synergistic effects and mechanism of multiwalled carbon nanotubes with magnesium hydroxide in halogen-free flame retardant EVA/MH/MWNT nanocomposites, Polymer Degradation and Stability, 94(5), 751-756.
22.DINTCHEVA, N. T., ARRIGO, R., MORREALE, M., LA MANTIA, F. P., MATASSA, R., CAPONETTI, E., (2011), Effect of elongational flow on morphology and properties of polymer/CNTs nanocomposite fibers, Polymers for Advanced Technologies, 22(12), 1612-1619.
23.LOZANO-PÉREZ, C., CAUICH-RODRÍGUEZ, J. V., AVILÉS, F., (2016), Influence of rigid segment and carbon nanotube concentration on the cyclic piezoresistive and hysteretic behavior of multiwall carbon nanotube/segmented polyurethane composites, Composites Science and Technology, 128, 25-32.
24.QU, M., QIN, Y., SUN, Y., XU, H., SCHUBERT, D. W., ZHENG, K., ... NILSSON, F., (2020), Biocompatible, flexible strain sensor fabricated with polydopamine-coated nanocomposites of nitrile rubber and carbon black, ACS Applied Materials & Interfaces, 12(37), 42140-42152.

25.LIU, H., LI, Q., BU, Y., ZHANG, N., WANG, C., PAN, C., ... SHEN, C., (2019)., Stretchable conductive nonwoven fabrics with self-cleaning capability for tunable wearable strain sensor, Nano Energy, 66, 104143.
26.STARÝ, Z., KRÜCKEL, J., WECK, C., SCHUBERT, D. W., (2013), Rheology and conductivity of carbon fibre composites with defined fibre lengths, Composites science and technology, 85, 58-64.
27.QU, M., SCHUBERT, D. W., (2016), Conductivity of melt spun PMMA composites with aligned carbon fibers, Composites Science and Technology, 136, 111-118.
28.DUAN, L., FU, S., DENG, H., ZHANG, Q., WANG, K., CHEN, F., FU, Q., (2014), The resistivity–strain behavior of conductive polymer composites: stability and sensitivity, Journal of Materials Chemistry A, 2(40), 17085-17098.
29.QU, M., QIN, Y., XU, W., ZHENG, Z., XU, H., SCHUBERT, D. W., GAO, Q., (2021), Electrically conductive NBR/CB flexible composite film for ultrastretchable strain sensors: Fabrication and modeling, Applied Nanoscience, 11, 429-439.
30.LI, S., GAO, W., ZHANG, Q., JIANG, Z., CHEN, L., (2022), The Strain Sensoring Behavior of the Melt-extruded Ethylene-vinyl Acetate (EVA)/carbon Black Composites Filament, *Mater. Plast.*, **59**(4), 165-176.
31.XIANG-WU ZHANG, PAN, Y., ZHENG, Q., XIAO-SU YI, (2000), Time dependence of piezoresistance for the conductor-filled polymer composites, Journal of Polymer Science Part B: Polymer Physics, 38(21).
32.SIMMONS, J. G., (1963), Generalized formula for the electric tunnel effect between similar electrodes separated by a thin insulating film, Journal of applied physics, 34(6), 1793-1803.
33.ZHANG, X. W., PAN, Y., ZHENG, Q., YI, X. S., (2000), Time dependence of piezoresistance for the conductor-filled polymer composites, Journal of Polymer Science part B: polymer physics, 38(21), 2739-2749.
34.ZHENG, Y., LI, Y., LI, Z., WANG, Y., DAI, K., ZHENG, G., ... SHEN, C., (2017), The effect of filler dimensionality on the electromechanical performance of polydimethylsiloxane based conductive nanocomposites for flexible strain sensors, Composites Science and Technology, 139, 64-73.
35.GONG, S., SCHWALB, W., WANG, Y., CHEN, Y., TANG, Y., SI, J., ... CHENG, W., (2014), A wearable and highly sensitive pressure sensor with ultrathin gold nanowires, Nature communications, 5(1), 3132.
36.QU, M., LI, D., QIN, T., LUO, Z., LIU, X., NILSSON, F., ... QIN, Y., (2022), Carbon Black Nanoparticle/Polydopamine-Coated Core-Spun Yarns for Flexible Strain Sensors, ACS Applied Nano Materials, 5(11), 16996-17003.
37.LIU, Z., LI, Z., ZHAI, H., JIN, L., CHEN, K., YI, Y., ... ZHENG, Z., (2021), A highly sensitive stretchable strain sensor based on multi-functionalized fabric for respiration monitoring and identification, Chemical Engineering Journal, 426, 130869.

Manuscript received: 2.08.2023